

Bi_2Te_3 : Implications of the rhombohedral \mathbf{k} -space texture on the evaluation of the in-plane/out-of-plane conductivity anisotropy

Peter Zahn, Nicki F. Hinsche, and Bogdan Yavorsky

Institut für Physik, Martin-Luther-Universität Halle-Wittenberg, D-06099 Halle, Germany

Ingrid Mertig

*Institut für Physik, Martin-Luther-Universität Halle-Wittenberg, D-06099 Halle, Germany and
Max-Planck-Institut für Mikrostrukturphysik, Weinberg 2, D-06120 Halle, Germany*

(Dated: October 15, 2018)

Different computational scheme for calculating surface integrals in anisotropic Brillouin zones are compared. The example of the transport distribution function (plasma frequency) of the thermoelectric Material Bi_2Te_3 near the band edges will be discussed. The layered structure of the material together with the rhombohedral symmetry causes a strong anisotropy of the transport distribution function for the directions in the basal (in-plane) and perpendicular to the basal plane (out-of-plane). It is shown that a thorough reciprocal space integration is necessary to reproduce the in-plane/out-of-plane anisotropy. A quantitative comparison can be made at the band edges, where the transport anisotropy is given in terms of the anisotropic mass tensor.

PACS numbers: 71.18.+y, 71.20.Gj, 72.20.Pa, 72.80.Jc

I. INTRODUCTION

Thermoelectric materials are nowadays widely used to convert waste heat into electrical energy or for cooling purposes.¹ The main advantage of this conversion process is the absence of moving parts or liquid or gaseous components. The efficiency of the process is rather low and is mainly determined by the dimensionless parameter

$$ZT = \frac{\sigma S^2}{\kappa} \quad ,$$

called figure of merit. It is determined by the specific conductivity σ , the thermopower S , the absolute temperature T , and the thermal conductivity κ , comprising the electronic and lattice parts κ_e and κ_L .

New experimental techniques allow for the preparation of nanostructured and low-dimensional thermoelectric devices which are supposed to possess larger ZT values.^{2,3} Values up to 2.4 are reported for multilayered $\text{Bi}_2\text{Te}_3/\text{Sb}_2\text{Te}_3$ systems.^{4,5} A microscopic understanding of these effects can be obtained by calculating the conductivity and powerfactor in the semi-classical limit exploiting the relaxation time approximation. The so-called transport distribution function has to be determined as a function of electron energy E as integrals of surfaces of constant electron energy in reciprocal space.⁶ If one considers an anisotropic material, like Bi_2Te_3 , these quantities show a strong directional dependence, which can support the enhancement of figure of merit in thermoelectric heterostructures. The calculation of these isoenergetic surface integrals requires a

thorough integration in \mathbf{k} space. The implications of different integration scheme will be demonstrated. To this end the paper is organized as follows. We start with a derivation of the transport anisotropy near the band edges as a function of the effective mass tensor. This provides benchmark numbers at certain energies to check the numerical integration schemes. The systematic deviations of the integration schemes are related to the anisotropic structure of the reciprocal space of the rhombohedral lattice and the anisotropy of the band edges concerning the effective masses are discussed afterwards. At the end, a simplified analytical model for a two-dimensional integration will be discussed to show the influence of the rhombohedral lattice anisotropy on the transport quantities. Results for a free electron model show a strong dependence on the procedure to fill the reciprocal space with tetrahedrons in a way that the symmetry operations of the lattice can still be applied to reduce the numerical effort.

II. INVERSE MASS TENSOR AND CONDUCTIVITY ANISOTROPY AT BAND EDGES

We determined the band dispersion for Bi_2Te_3 at the experimental lattice constants with the atomic positions taken from literature.⁷ The topology of the band structure is described elsewhere.⁸ Assuming a constant relaxation time the energy dependent matrix valued transport distribution is defined as⁶

$$\sigma_{\alpha\beta}(E) = \tau \frac{e^2}{(2\pi)^3 \hbar} \int_{\epsilon(k)=E} \frac{dS}{|\vec{v}(k)|} v_\alpha(k) v_\beta(k) \quad , \quad (1)$$

with α, β the Cartesian coordinates, k a combined index of reciprocal space vector \vec{k} and band index ν , $\epsilon(k)$ the band energy, and $v_\alpha(k)$ the group velocity in the direction α . To obtain the anisotropy σ_{xx}/σ_{zz} as a point of reference, we assume in the vicinity of the band edges parabolic bands in an anisotropic effective mass model. The inverse mass tensor \underline{M} close to the band edges is diagonalized in the form

$$\underline{M} = \underline{m}^{-1} = \text{diag}(M_1, M_2, M_3), \quad \text{with eigenvectors} \\ \vec{c}_i = c_{i,x}\vec{e}_x + c_{i,y}\vec{e}_y + c_{i,z}\vec{e}_z \quad (i = 1 \dots 3) \quad , \quad (2)$$

with \vec{e}_α the basis vectors of the Cartesian coordinate system. The transport distribution for the anisotropic effective mass model along the main axes \vec{c}_i of the effective mass ellipsoid are proportional to

$$\sigma_{ii} \propto \frac{\sqrt{m_1 m_2 m_3}}{m_i} \quad (3)$$

$$\propto \frac{\bar{m}}{m_i} = \bar{m} M_i \quad \text{with} \\ \bar{m} = \sqrt{m_1 m_2 m_3} \quad , \quad (4)$$

where the masses have to be chosen positive for both the valence band maximum and the conduction band minimum.

The following expressions for the in-plane and cross-plane conductivities project the mass tensor of general orientation given by eq. (2) to the Cartesian coordinates.

$$\sigma_{xx} \propto \vec{e}_x^T \underline{M} \vec{e}_x \\ \propto (c_{1,x})^2 M_1 + (c_{2,x})^2 M_2 + (c_{3,x})^2 M_3 \\ \sigma_{yy} \propto (c_{1,y})^2 M_1 + (c_{2,y})^2 M_2 + (c_{3,y})^2 M_3 \\ \sigma_{zz} \propto (c_{1,z})^2 M_1 + (c_{2,z})^2 M_2 + (c_{3,z})^2 M_3 \quad (5)$$

Due to the space group $D_{3d}^5 (R\bar{3}m)$ the considered band extrema are two- and six-fold degenerate. In the case of the rhombohedral lattice this summation leads to equal contributions σ_{xx} and σ_{yy} and keeps the σ_{zz} unchanged. The in-plane transport distribution is given for symmetry reasons by $\sigma_{\parallel} = (\sigma_{xx} + \sigma_{yy})/2$. and the cross-plane component by $\sigma_{\perp} = \sigma_{zz}$. In the following the term σ_{xx} will be used synonymously for the in-plane component σ_{\parallel} , so the anisotropy is denoted as σ_{xx}/σ_{zz} .

The mass tensor in Bi_2Te_3 is parameterized close to the band edges using the calculated

band structure on a very dense mesh in k -space corresponding to 400 points along a reciprocal lattice vector to obtain convergence concerning the position of the extremum and the inverse mass tensor. The values for the valence and the conduction band are summarized in Tabs. I. and II.⁸

VBM	M_i	$c_{i,x}$	$c_{i,y}$	$c_{i,z}$
1	-41.3	0.5000	-0.8660	0.0000
2	-7.42	0.6000	0.3463	0.7212
3	-0.507	0.6246	0.3606	-0.6927

TABLE I: Inverse effective mass tensor eigenvalues M_i and eigenvectors \vec{c}_i at the valence band maximum (VBM).

The position \vec{q}_S of the six-fold degenerate valence band maximum in units of inverse Bohr radii is (0.372199, 0.644655, -0.0299675) on the plane (ΓZU). The effective mass ellipsoid is very anisotropic. The angle ϕ of the long axis of the ellipsoid with the (xy) basal plane is 43.8° , which is in good agreement to other calculations and experiments, which show a quite spread.⁹⁻¹¹ The transport anisotropy ratio determined by the effective mass tensor for hole states close to the valence band maximum accounts to $\sigma_{xx}/\sigma_{zz} = 5.40$.

CBM	M_i	$c_{i,x}$	$c_{i,y}$	$c_{i,z}$
1	5.62	1.	0.	0.
2	5.62	0.	1.	0.
3	1.20	0.	0.	1.

TABLE II: Inverse effective mass tensor eigenvalues M_i and eigenvectors \vec{c}_i at the Conduction band minimum (CBM).

Tab. II summarizes the effective mass tensor at the two-fold degenerate conduction band minimum with a the position \vec{q}_S in units of inverse Bohr radii (0,0,0.0552), which is about one third of the line(ΓZ). The transport anisotropy is $\sigma_{xx}/\sigma_{zz} = 4.67$.

With these values the convergence of the transport distribution given by eq. (1) determined by interpolation schemes in the Brillouin zone for energies close to the band edges can be quantified.

Using the calculated band structures and the derived effective mass tensors we obtain an anisotropy σ_{xx}/σ_{zz} of 5.40 and 4.67 at the valence and conduction band edge, respectively. These values are marked by dots in Figs. 1) and 2).

III. CONDUCTIVITY ANISOTROPY: COMPARISON OF DIFFERENT INTERPOLATION SCHEME

The transport distribution $\sigma(E)$ of Bi_2Te_3 is calculated by two methods. The main distinction is the determination of the group velocities $\vec{v}(k)$.

The tetrahedron method divides the irreducible part of the Brillouin Zone (BZ) into disjoint tetrahedra. The group velocity is obtained by a linear interpolation of the band energies at the 4 corner points and approximates $\vec{v}(k)$ in the volume of the tetrahedron.¹² The second method determines the velocities as derivatives along the lines of the Blöchl mesh¹³ in the whole Brillouin zone. The directions of these lines are parallel to the reciprocal space vectors and so the anisotropy of the real lattice is reflected in these vectors. For Bi_2Te_3 with a large ratio $c^{\text{hex}}/a^{\text{hex}}$ of 6.95⁷ the real space unit cell is very prolonged and the reciprocal lattice vectors are quite close to the (xy) basal plane with an angle $\theta' = 118.05^\circ$ between them very close to the maximum value of 120° . Projecting back these so-called mesh velocities to the Cartesian components quite large errors occur in the resulting velocities as discussed below. The results of the integration of eq. (1) using both interpolations schemes and different densities of k-points are compared in Figs. 1) and 2).

We start the discussion with the valence band maximum because the principal axes of the mass tensor are directed along the x, y and z axis. The left hand panel of Fig. 1 shows the parabolic dispersion along the three principal axes with the very different effective masses, spreading by a factor of about 80. The right hand panel summarizes the anisotropy ratios σ_{xx}/σ_{zz} as a function of energy. It is obvious that both interpolation schemes give systematic deviations from the expected values. For very large k-mesh densities defined by 384 mesh points along a reciprocal lattice vector the results converge to the correct value at the band edge. The necessary densities of k-points are very demanding for realistic band structure calculations with some atoms in the unit cell. The tetrahedron method overestimates systematically the anisotropy ratio, whereas the mesh velocity method underestimates the values. This behavior will be discussed below for a simpler two-dimensional lattice and the found trends are confirmed.

A similar behavior is obtained for the conduction band minimum as shown in Fig. 2). Here, a second challenge appears with a local maximum

of the conduction band at the Γ point very close in energy to the conduction band minimum. In addition, a large transport anisotropy is obtained due to the occurrence of saddle points in the band structure, as discussed elsewhere.⁸

The obtained anisotropies for the transport distribution can be strongly influenced by the k-mesh density especially close to the band edges. Taking the converged transport distributions $\Sigma(E)$ we obtained for small p-doping an anisotropy of about 6, and for small n-doping an anisotropy of about 9.¹⁴ This about a factor of 2 larger than found in experiment¹⁵ and other calculations.^{16–18} Assuming an anisotropy of 0.47 for the averaged relaxation time of states traveling along and across the basal plane we obtain a good agreement with experiment. The reason for this scattering anisotropy has to be elucidated by calculations of the microscopic transition probabilities caused by defects or other scattering centers.

IV. INTERPOLATION SCHEMES: TETRAHEDRON VS. MESH VELOCITIES

A. Mesh velocity method

In the following the implications of the different interpolation schemes for the group velocity are discussed. We start with the discussion of the so-called mesh velocities. They are determined by a numerical derivative of the band dispersion along the directions of the reciprocal lattice vectors which span the Blöchl mesh. The Cartesian components of the velocities are obtained by a non-orthogonal transformation. If the angles between the basis vectors are very large (the maximum is 120°) small errors can be largely enhanced. This appears especially at band structures with a strong anisotropy between directions in (xy)-plane and the z-direction.

Fig. 3 shows schematically the band dispersion of Bi_2Te_3 close to the conduction band minimum by isoenergetic lines. The Brillouin zone is shown in reduced size but the angles correspond to the considered case of Bi_2Te_3 . As it is obvious, the interpolation of the velocities deviates strongly from the correct values for k-points close to the band extremum. The directions of the reciprocal basis vector mainly scan along the (xy)-plane. If the anisotropy of the band dispersion $\epsilon(k)$ is very strong as in the case considered, the mesh velocities tend to equalize the in-plane and out-of-plane com-

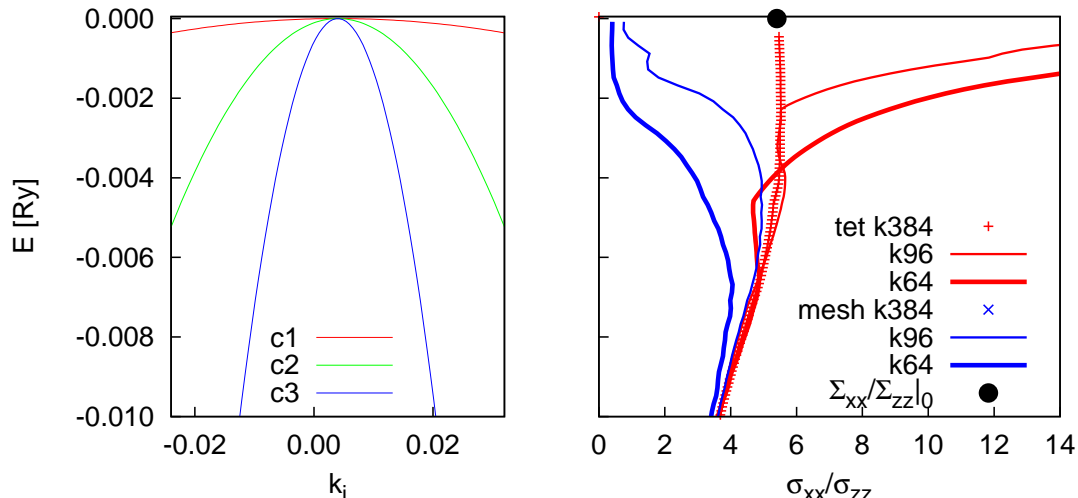


FIG. 1: Band structure of Bi_2Te_3 (left) and conductivity ratio (right) near valence band maximum, group velocity interpolation by tetrahedron method (tet) and mesh velocity concept (mesh), number of k-points along a reciprocal lattice vector is given as parameter. Observe that the vertical axis gives the energy and the anisotropy σ_{xx}/σ_{zz} is on the horizontal axis.

ponents of the velocity $v_{x,y} \approx v_z$ which leads to an anisotropy closer to unity. This can be seen in Figs. 1) and 2) by the curves labeled 'mesh'. This effect is most pronounced close to the band edges.

A quantitative comparison of the accuracy of the mesh velocities is given in fig. 4. To compare the mesh velocities with the exact values we have chosen the ΓZ line and consider the z-component of the velocity $v_z(k_z)$. The minimum of the energy dispersion is the global minimum of the conduction band. A local maximum appears at the Γ point. For sparse k-mesh densities a strong deviation of the mesh velocities have to be stated. To reproduce the point of inflection of the band dispersion by the sign change in the velocity a very dense mesh is necessary. The velocity in z-direction is overestimated by this method, if the velocities in the (xy) directions are larger than in z-direction, as illustrated in fig. 3 and typical for Bi_2Te_3 in both the valence and conduction band. As a result the transport anisotropy σ_{xx}/σ_{zz} , which is de facto the ratio of the velocities squared, is shifted to unity. An increase of the anisotropy towards 1 is expected for the opposite case with

larger velocities along z-direction than along (xy) directions.

B. Tetrahedron method

The capability of the tetrahedron method to calculate the anisotropy of the transport distribution will be evaluated for a two-dimensional mesh for the cases of linear and quadratic interpolation of the velocities. The results for a free electron dispersion with two different arrangements of tetrahedrons in the irreducible part of a three-dimensional meshes will be compared with.

The regular filling of the two-dimensional lattice is characterized by the angle α between the border line of the triangles S_1 and S_2 and the basal (xy)-plane, see Fig. 5. Depending on the interpolation method the velocities have to be determined for the triangles S_1 and S_2 with a linear scheme and can be determined at the points A, B, and C with a quadratic interpolation scheme. The second task requires the knowledge of the energy dispersion $\epsilon(k)$ at additional points on the edges. Solving the lin-

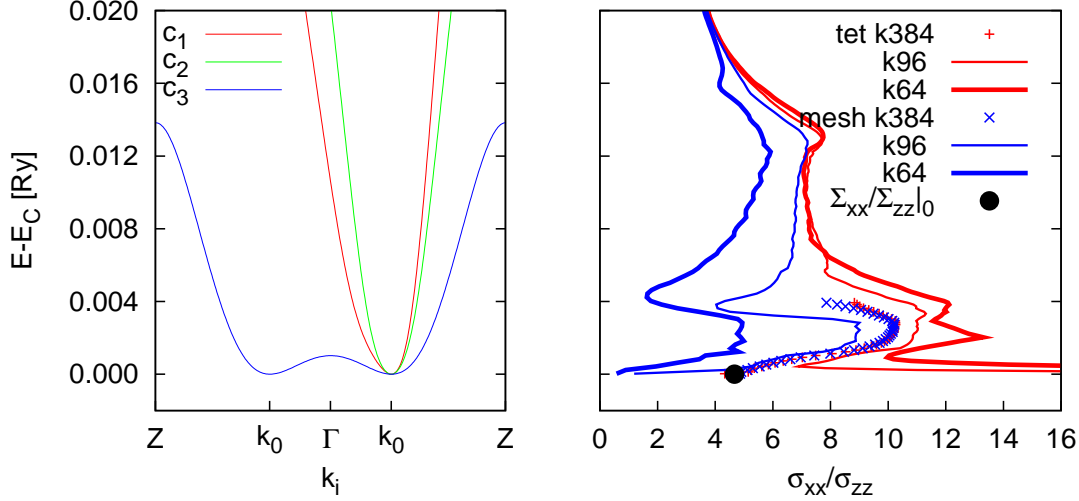


FIG. 2: Band structure of Bi_2Te_3 (left) and conductivity ratio (right) near conduction band minimum. see fig. 1

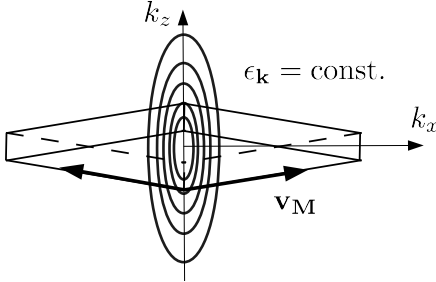


FIG. 3: Determination of the group velocity by means of so-called mesh velocities v_M along the reciprocal basis vectors. Anisotropic band dispersion is sketched by elliptical isoenergetic lines $\epsilon_k = \text{const.}$ in the (k_x, k_z) -plane. The rhombohedral Brillouin zone for the case of Bi_2Te_3 is shown by thin lines.

ear set of equations for the Cartesian components of the velocities \vec{v}_1 and \vec{v}_2 for a free electron dispersion, one finds both velocities equal pointing in the same direction along the borderline of the two triangles $\vec{v}_1 \parallel \vec{v}_2 \parallel (\cos \alpha, \sin \alpha)$. So, the anisotropy of the transport distribution σ_{xx}/σ_{zz} is just given by the ratio of the components v_x and v_z squared

$$\sigma_{xx}/\sigma_{zz} = \frac{\cos^2 \alpha}{\sin^2 \alpha} = \frac{1}{\tan^2 \alpha} \quad (6)$$

For the given c/a ratio of Bi_2Te_3 the angle α is about 23° which results an anisotropy value of 5.8 which is much too large in comparison of the expected unity ratio. Improving the interpolation scheme of the velocity to second order the velocities \vec{v}_A , \vec{v}_B , and \vec{v}_C are determined correctly and the error of the transport distribution function is mainly determined by the approximation of the Fermi surface (a line in the two-dimensional case) by the two line segments a_1 and a_2 . Due to the canceling of prefactors in the ratio σ_{xx}/σ_{zz} it is sufficient to consider the sum of the segment lengths $|a_1|$ and $|a_2|$ times the square of the corresponding velocity components of \vec{v}_A and \vec{v}_B for area S_1 , and \vec{v}_B and \vec{v}_C for area S_2 , see eq. (1)

$$\begin{aligned} \sigma_{xx} &\propto \cos^2 \alpha \sqrt{(1 - \sin^2 \alpha)^2 + \cos^2 \alpha} + \\ &\quad + (1 + \cos^2 \alpha) \sqrt{(1 - \cos^2 \alpha)^2 + \sin^2 \alpha} \\ &\propto \cos^2 \alpha \sqrt{2 - 2 \sin \alpha} + (1 + \cos^2 \alpha) \sqrt{2 - 2 \cos \alpha} \\ \sigma_{zz} &\propto \sin^2 \alpha \sqrt{2 - 2 \sin \alpha} + (1 + \sin^2 \alpha) \sqrt{2 - 2 \cos \alpha} \quad (7) \end{aligned}$$

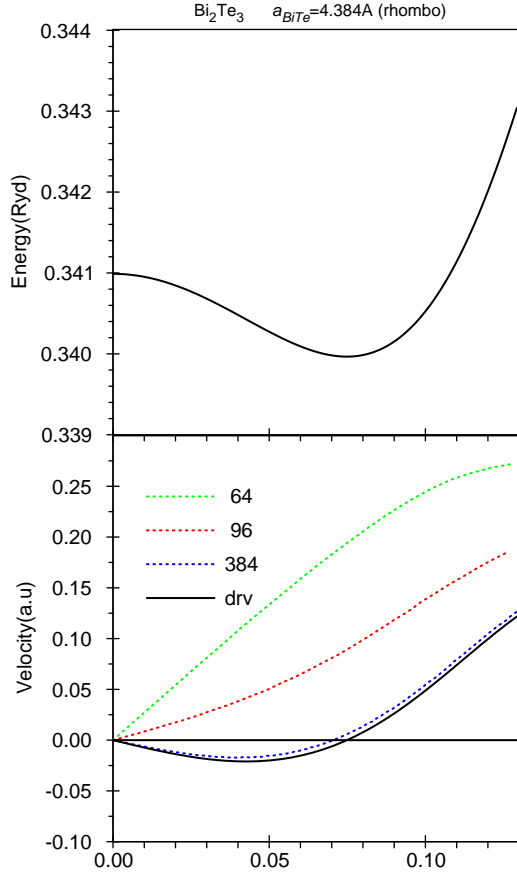


FIG. 4: Band structure $\epsilon(k_z)$ of Bi_2Te_3 on the line Γ -Z (top) and mesh velocities in z direction (bottom) for different densities of the k -mesh. 'drv' denotes the exact result from the derivate $\partial\epsilon(k_z)/\partial k_z$.

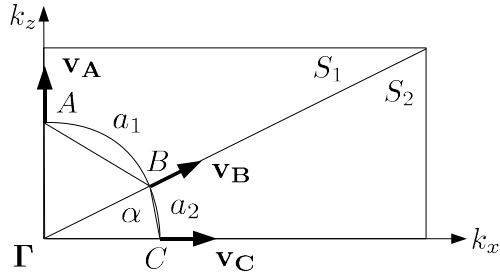


FIG. 5: Schematic sketch of an anisotropic k -mesh division characterized by the angle α . The constant energy surface is approximated by the polygon ABC with the parts a_1 and a_2 in the triangles S_1 and S_2 . \vec{v}_A , \vec{v}_B , and \vec{v}_C denote the velocities.

From these expressions the ration σ_{xx}/σ_{zz} is evaluated and shown as (thicker) blue lines in fig. 5 together with the values obtained by the linear velocity interpolation as (thinner) red lines. The linear scheme shows strong devi-

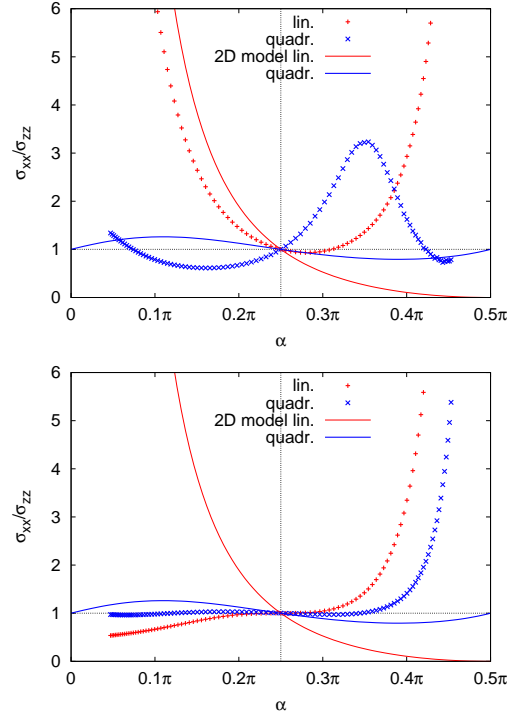


FIG. 6: Anisotropy of conductivity for a free electron model in dependence of the assumed underlying rhombohedral lattice characterized by the angle α between the reciprocal lattice vectors and the (xy) basal plane. As comparison the conductivity anisotropies of the 2D model (linear and quadratic interpolation) are shown with solid lines. Top panel: k -mesh created along $(11\bar{1})$ directions, bottom panel: k -mesh created along (001) directions.

ations especially for very anisotropic lattices with small or large angles α . This error is much reduced by the second order interpolation scheme with a maximum error of about 30%.

Performing these procedures in a three-dimensional lattice requires the set-up of k -point mesh filling the irreducible part of the Brillouin zone and allowing for a disjunct tetrahedron arrangement. Two filling schemes are evaluated, which are based on cubes (in a given basis) which are filled with 6 tetrahedron each if completely inside the irreducible part, otherwise they are partially used to fill the irreducible part. The first one is based on cubes with the main axes directed along the $(11\bar{1})$ reciprocal lattice directions. The results for the anisotropy σ_{xx}/σ_{zz} with a linear and a quadratic velocity interpolation are shown as crosses and plus signs in the upper panel of fig. 6, respectively. To define a similar angle \angle characterizing the anisotropy of the rhombohedral reciprocal lattice as in the two-dimensional

case we have chosen $(\pi - \angle(\vec{g}_1, \vec{g}_2 + \vec{g}_3))/2$ to ensure the isotropic simple cubic lattice to be characterized by an angle $\pi/4$.

The second filling scheme uses the (001) directions as basis. The results are shown in the lower panel of fig. 6. The results of the two-dimensional model can be partially reproduced, especially the case of a isotropic lattice at an angle of 45° . On average the deviations are larger for the linear interpolation scheme in comparison to the quadratic one as expected from the two-dimensional model. The partially opposite behaviour of the three-dimensional integration scheme with respect to the two-dimensional one needs further clarifications.

The results in fig. 6 are evaluated for energies very close to the free electron band minimum. In these cases the isoenergetic surface is approximated by a few trigonal elements only and the largest anisotropies caused by the interpolation errors of velocities and surface areas are expected. For larger energies these discrepancies disappear quickly. The discussed deficiencies of the interpolation schemes

in k-space are restricted to energies close to band extrema, which appear in transport properties of medium-doped semiconductors. In cases of very small doping the application of an anisotropic effective mass model seems to be more advantageous.

V. CONCLUSIONS

By means of model and realistic band structure calculations for crystals with rhombohedral symmetry we have shown that the determination of the transport distribution function requires very dense meshes in k-space. Two different methods to determine the group velocities are evaluated. It is found that they underestimate and overestimate the transport anisotropy in a systematic manner. For very prolonged unit cells the anisotropy in k-space requires a thorough check of the convergence with respect to k-space density.

¹ F. J. DiSalvo, *Science* **285**, 703 (1999).

² L. D. Hicks and M. S. Dresselhaus, *Phys. Rev. B* **47**, 12727 (1993).

³ L. D. Hicks and M. S. Dresselhaus, *Phys. Rev. B* **47**, 16631 (1993).

⁴ R. Venkatasubramanian, T. Colpitts, B. O'Quinn, S. Liu, N. El-Masry, and M. Lamvik, *Appl. Phys. Lett.* **75**, 1104 (1999).

⁵ R. Venkatasubramanian, E. Siilova, T. Colpitts, and B. O'Quinn, *Nature* **413**, 597 (2001).

⁶ G. Mahan and J. Sofo, *Proc. Nat. Acad. Sci.* **93**, 7436 (1996).

⁷ R. Clasen, P. Grosse, A. Krost, F. Levy, S. Marenkin, W. Richter, N. Ringelstein, R. Schmechel, G. Weiser, H. Werheit, et al., in *Landolt-Börnstein, New Series, Volume III/41C*, edited by O. Madelung (Springer-Verlag, Berlin, 1998).

⁸ B. Y. Yavorsky, N. F. Hinsche, I. Mertig, and P. Zahn, *subm. to PRB (MS BG12124)* (2011).

⁹ S. K. Mishra, S. Satpathy, and O. Jepsen, *J.*

Phys. Cond. Matter **9**, 461 (1997).

¹⁰ H. Köhler, *Phys. Stat. sol. B* **73**, 95 (1976).

¹¹ M. Stordeur, M. Stölzer, H. Sobotta, and V. Riedle, *Phys. Stat. sol. B* **150**, 165 (1988).

¹² G. Lehmann and M. Taut, *Phys. Stat. sol. B* **54**, 469 (1972).

¹³ P. Blöchl, O. Jepsen, and O. Andersen, *Phys. Rev. B* **49**, 16223 (1994).

¹⁴ N. F. Hinsche, B. Yavorsky, I. Mertig, and P. Zahn, *subm. to PRB (MS BG12149)* (2011).

¹⁵ R. T. Delves, A. E. Bowley, D. W. Hazelden, and H. J. Goldsmid, *Proc. Phys. Soc.* **78**, 838 (1961).

¹⁶ T. J. Scheidemantel, C. Ambrosch-Draxl, T. Thonhauser, J. V. Badding, and J. O. Sofo, *Phys. Rev. B* **68**, 125210 (2003).

¹⁷ B.-L. Huang and M. Kaviani, *Phys. Rev. B* **77**, 125209 (2008).

¹⁸ M. S. Park, J.-H. Song, J. E. Medvedeva, M. Kim, I. G. Kim, and A. J. Freeman, *Phys. Rev. B* **81**, 155211 (2010).